Engineering Material Properties of Transcription Factor Condensates to Control Gene Expression in Mammalian Cells and Mice

*Alexandra A.M. Fischer, Deqiang Kong, Merlin M. Grimm, Jakob Grether, Johanna Groth, Manfred Fliegauf, Bodo Grimbacher, Haifeng Ye, Wilfried Weber**

Alexandra A.M. Fischer, Merlin M. Grimm, Jakob Grether, Johanna Groth, Wilfried Weber
Signalling Research Centres BIOSS and CIBSS
University of Freiburg
Schänzlestraße 18, 79104 Freiburg, Germany
E-mail: Wilfried.Weber@leibniz-inm.de

Alexandra A.M. Fischer, Merlin M. Grimm, Jakob Grether, Johanna Groth, Wilfried Weber
Faculty of Biology
University of Freiburg
Schänzlestraße 18
79104 Freiburg, Germany.

Alexandra A.M. Fischer, Wilfried Weber
Spemann Graduate School of Biology and Medicine (SGBM)
University of Freiburg
Albertstraße 21a
79104 Freiburg, Germany

Alexandra A.M. Fischer, Wilfried Weber
INM – Leibniz Institute for New Materials
Campus D2 2
66123 Saarbrücken, Germany

Wilfried Weber
Saarland University
Department of Materials Science and Engineering
Campus D2 2
66123 Saarbrücken, Germany

Deqiang Kong, Haifeng Ye
Synthetic Biology and Biomedical Engineering Laboratory
Biomedical Synthetic Biology Research Center
Shanghai Key Laboratory of Regulatory Biology
Institute of Biomedical Sciences and School of Life Sciences
East China Normal University
Dongchuan Road 500
Shanghai 200241, China.

Jakob Grether
Biberach University of Applied Sciences
Karlstraße 6-11
Biberach an der Riß, Germany

Manfred Fliegauf, Bodo Grimbacher
Institute for Immunodeficiency
Center for Chronic Immunodeficiency (CCI)
Medical Center, Faculty of Medicine
University of Freiburg
Breisacherstr. 115
79106 Freiburg, Germany

Bodo Grimbacher
DZIF – German Center for Infection Research
Satellite Center Freiburg
Breisacherstr. 115
79106 Freiburg, Germany

Bodo Grimbacher
RESIST – Cluster of Excellence 2155 to Hanover Medical School
Satellite Center Freiburg
Breisacherstr. 115
79106 Freiburg, Germany

Manfred Fliegauf, Bodo Grimbacher

CIBSS – Centre for Integrative Biological Signalling Studies, University of Freiburg, Schänzlestraße 18, 79104 Freiburg, Germany.

Keywords: material properties of protein condensates, biomolecular condensates, protein co-acervates, synthetic biology

Abstract

Phase separation of biomolecules into condensates is a key mechanism in the spatiotemporal organization of biochemical processes in cells. However, the impact of the material properties of biomolecular condensates on important processes, such as the control of gene expression, remains largely elusive. Here, we systematically tune the material properties of optogenetically induced transcription factor condensates and probe their impact on the activation of target promoters. We demonstrate that rather liquid condensates correlate with increased gene expression levels, whereas a gradual transition to more stiff condensates converts otherwise activating transcription factors into dominant negative inhibitors. We demonstrate the general nature of these findings in mammalian cells and mice, as well as by using different synthetic and natural transcription factors. We observe these effects for both transgenic and cell-endogenous promoters. Our findings provide a novel materials-based layer in the control of gene expression, which opens novel opportunities in (opto-)genetic engineering and synthetic biology.

1. Introduction

Biomolecular condensates enable the spatial and temporal organization of cellular reactions by serving as compartments that partition molecules rapidly and selectively through phase separation.[1,2] Recent approaches to design biomolecular condensates have inspired a new generation of synthetic biology strategies to influence cell fate and function or to elucidate basic biological principles that rely on phase separation.[3] Examples include the spatially controlled incorporation of synthetic amino acids into protein polymers,[4] the control over *E.coli* biochemistry by sequestration of pathways or buffering of mRNA translation rates,[5] the design of biochemical reaction centers to re-route molecular fluxes,[6] the 3D organization of macromolecular complexes controlling genome architecture,[7] epigenetic imprinting,[8] or the modulation of gene expression.[9,10]

Key driving forces for biomolecular condensate formation are the concentration of the involved molecules (such as proteins, RNA, or DNA), the biophysical properties of the involved biopolymers, as well as the multivalent interactions among them. Multivalency is often given through intrinsically disordered regions (IDRs) which are stretches of amino acids without any specific secondary structure. Proteins such as FUS[11,12] or HNRNPA1[13] are well-known examples, described to undergo phase separation upon reaching a critical threshold concentration. Further,

an increase in the multivalency of IDR interaction, for example, through post-translational modifications or mutations, can promote transition from the liquid state to gel- or solid-like materials.[13–18]

Accordingly, the synthetic induction of multivalent interactions among IDRs enables the formation of biomolecular condensates on command. In a seminal study by the Brangwynne and Toettcher groups, the light-inducible homo-oligomerization of the *Arabidopsis thaliana* blue light photoreceptor Cry2 was used to increase the binding valency of IDRs and thus the formation of liquid protein condensates. By fusing IDRs to a mutant of Cry2, that forms higher-order oligomers ($Cry2_{olig}$), light-inducible solid-like gels were obtained, as measured by fluorescence recovery after photobleaching (FRAP). Further, as a function of the protein variant and the illumination conditions, the light-responsive formation of condensates with different material properties was observed.[19] Since then, light-inducible formation of condensates has been applied to elucidate fundamental mechanisms and functions of phase separation,[19,20] to optimize metabolic engineering,[6] or to amplify biomolecular processes such as transcription activation.[10]

Several recent studies have suggested that liquid-liquid phase separation (LLPS) of transcription factors plays important roles in the control of gene expression.[21–25] However, the reported effects of transcription factors undergoing LLPS range from positive[9,10,26,27] *via* neutral[28] to negative effects[29] on gene expression, with the underlying cause for this discrepancy remaining unknown. One possible mechanism that may have led to these divergent observations could be the different material properties of the investigated transcription factor condensates. Although it has been reported that material properties influence condensate function,[30–32] their influence on gene expression remains inconclusive.[33–36]

In this study, we systematically engineered light-inducible transcription factor condensates with different material properties and analyzed their influence on transcription activation in mammalian cells and mice. We first performed analysis of a synthetic transcription factor and subsequently generalized our findings by applying the same concept to selected natural transcription factors of the NF-κB, STAT3, and STAT6 pathways, that play pivotal roles in important processes like the immune response. We found that transcription factor condensates that exhibit rather liquid material properties have a positive effect on transgene expression levels, whereas stiffer condensates correlated with a decrease in the expression of synthetic reporter genes or endogenous promoters. Interestingly, the transformation of the transcription factor condensates into solid-like gels converted otherwise activating factors into dominant negative inhibitors of

transcriptional activity. These findings provide a novel, material-based concept of how biomolecular transcription factor condensates may influence gene expression. Furthermore, the molecular tools developed here may serve as an additional, material-based layer in synthetic biology for the control of target gene regulation.

2. Results

2.1. Engineering light-inducible transcription factor condensates with graded material properties

We hypothesized that altered material properties of transcription factor condensates may impact gene expression levels. To test this hypothesis, we used our previously established optogenetically-induced transcription factor condensates. This system is based on a split synthetic transcription factor comprising the DNA-binding domain TetR fused to CIBN (CIBN-TetR) and the activation domain VP16 fused to the blue light photoreceptor Cry2, further containing eYFP for visualization (Cry2-eYFP-VP16). In this configuration, illumination with blue light triggered dimerization of CIBN and Cry2 to reconstitute a functional transcription factor.[37] The incorporation of FUS_N-derived IDR (Cry2-eYFP-FUS_N-VP16) led to the formation of light-inducible liquid condensates due to Cry2 homo-oligomerization. The formation of liquid condensates at the promoter site correlated with up to 5-fold increased reporter gene expression compared to the non-condensed, IDR-lacking transcription factor[10]. This increase is most likely caused by the higher concentration of activation domains within the condensate in close vicinity to the promoter (Fig. 1A).[21]

In this study, we pursued two strategies to modulate the material properties of the transcription factor condensates: first, by selecting a mutant of Cry2 that correlates with enhanced clustering ($Cry2_{olig}$,[38] $Cry2_{olig}$-eYFP-FUS_N-VP16), and second, by gradually increasing the concentration of IDRs by modularly adding a construct encoding additional FUS_N fused to $Cry2_{olig}$ and mCherry (mCh, for visualization), by co-transfection. The construct further contained a nuclear localization sequence (NLS, $Cry2_{olig}$-mCh-FUS_N-NLS).

We transfected CIBN-TetR together with Cry2-eYFP-FUS_N-VP16 or $Cry2_{olig}$-eYFP-FUS_N-VP16 with or without additional $Cry2_{olig}$-mCh-FUS_N-NLS into HEK-293T cells together with a TetR-responsive reporter construct and observed immediate condensate formation upon blue-light illumination (Fig. 1B). We then analyzed the influence of the two strategies - $Cry2_{olig}$-enhanced clustering and increased IDR concentration - on condensate dynamics by conducting FRAP experiments. We recorded the recovery of photobleached condensates (Fig. 1B, S1) and compared the mobile fractions. Switching from Cry2 to Cry2olig led to a significantly smaller

(64% vs. 40%, respectively) mobile fraction, and the increase in IDR concentration by modular addition of Cry2$_{olig}$-mCh-FUS$_N$-NLS further decreased recovery to 17% for both Cry2-eYFP-FUS$_N$-VP16 and Cry2$_{olig}$-eYFP-FUS$_N$-VP16 (Fig 1B).

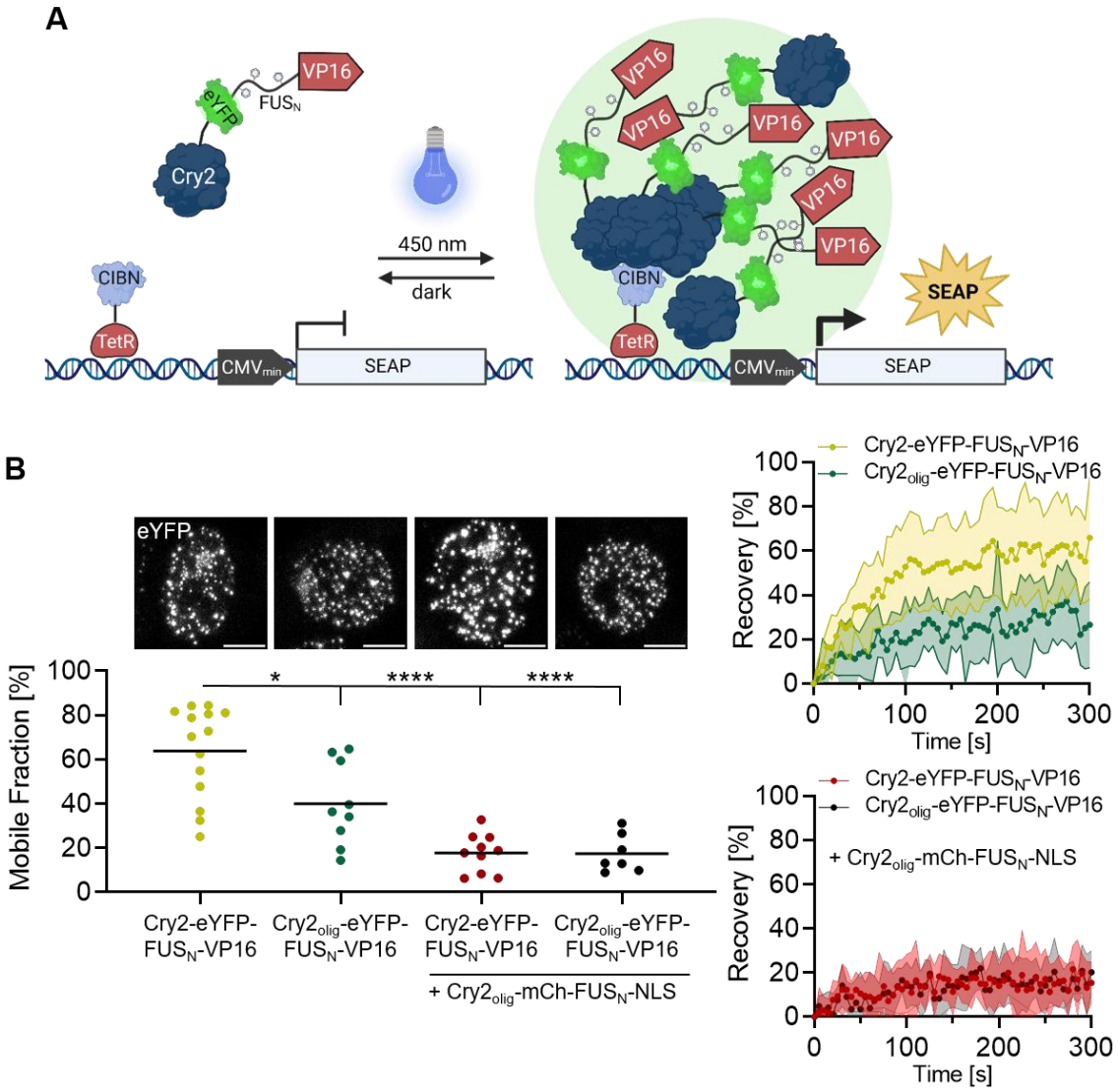

Figure 1. Design approach for tuning the material properties of transcription factor condensates. (**A**) Design of the light-dependent transcription factor. The transcription factor consists of two parts. First, a VP16 activation domain fused to the intrinsically disordered region (IDR) FUS$_N$, eYFP for visualization, and the blue light photoreceptor cryptochrome 2 (Cry2). Second, the DNA-binding motif TetR fused to CIBN. Upon illumination with blue light, Cry2 binds CIBN and further undergoes homo-oligomerization, leading to multivalent interactions and the induction of LLPS. VP16 is recruited to the transcription start site provided by the

CMV minimal promoter and induces reporter gene expression. (**B**) Tuning the material properties of transcription factor condensates. To modify condensate material properties, two strategies were pursued: first, increasing the valency of interaction by exchanging Cry2 for $Cry2_{olig}$, which forms higher-order oligomers; and second, increasing valency and concentration by co-transfection of a construct encoding $Cry2_{olig}$ fused to mCherry (for visualization) and FUS_N and a NLS. Constructs encoding CIBN-TetR and a $tetO_4$-based SEAP reporter were co-transfected into HEK-293T cells together with Cry2-eYFP-FUS_N-VP16 or $Cry2_{olig}$-eYFP-FUS_N-VP16 constructs (yellow and green data points). Optionally, the construct encoding $Cry2_{olig}$-mCh-FUS_N-NLS was added (in a 2:1 ratio in relation to the VP16-containing construct, red and black data points). The cells were cultivated in the dark for 32 h prior to FRAP analysis. FRAP measurements were started after 10 min of blue light illumination (2.5 µmol m^{-2} s^{-1}). Images show representative nuclei directly prior to droplet bleaching; scale bar = 5 µm. Graph shows the mean and single values of the mobile fractions calculated from the non-linear fits of $N \geq 7$ condensate recovery curves (see right panels). Pairwise comparisons were performed using a Student's t.test (* = $P < 0.05$; **** = $P < 0.0001$).

Complementarily, we analyzed condensate number per cell, area, integrated optical density (eYFP), and circularity (Fig. 2). Both Cry2-eYFP-FUS_N-VP16 and $Cry2_{olig}$-eYFP-FUS_N-VP16 yielded condensates of similar number and size. Upon addition of $Cry2_{olig}$-mCh-FUS_N-NLS, the condensate number per cell was significantly decreased and further diminished with increasing the amounts of this construct. Here, for the highest amount of $Cry2_{olig}$-mCh-FUS_N-NLS, a significant increase in condensate area was observed. The integrated optical density of eYFP (sum of all eYFP pixel values) in the condensates did not change significantly between the conditions, suggesting similar amounts of the eYFP-containing activation domains in all conditions. With increasing amounts of $Cry2_{olig}$-mCh-FUS_N-NLS, we observed a dose-dependent decrease of the condensate circularity. This finding is in agreement with previous observations that liquid condensates adapt spherical shapes, whereas increasing immobile fractions are correlated with more irregular shapes (Fig. 2B).[19,39,40]

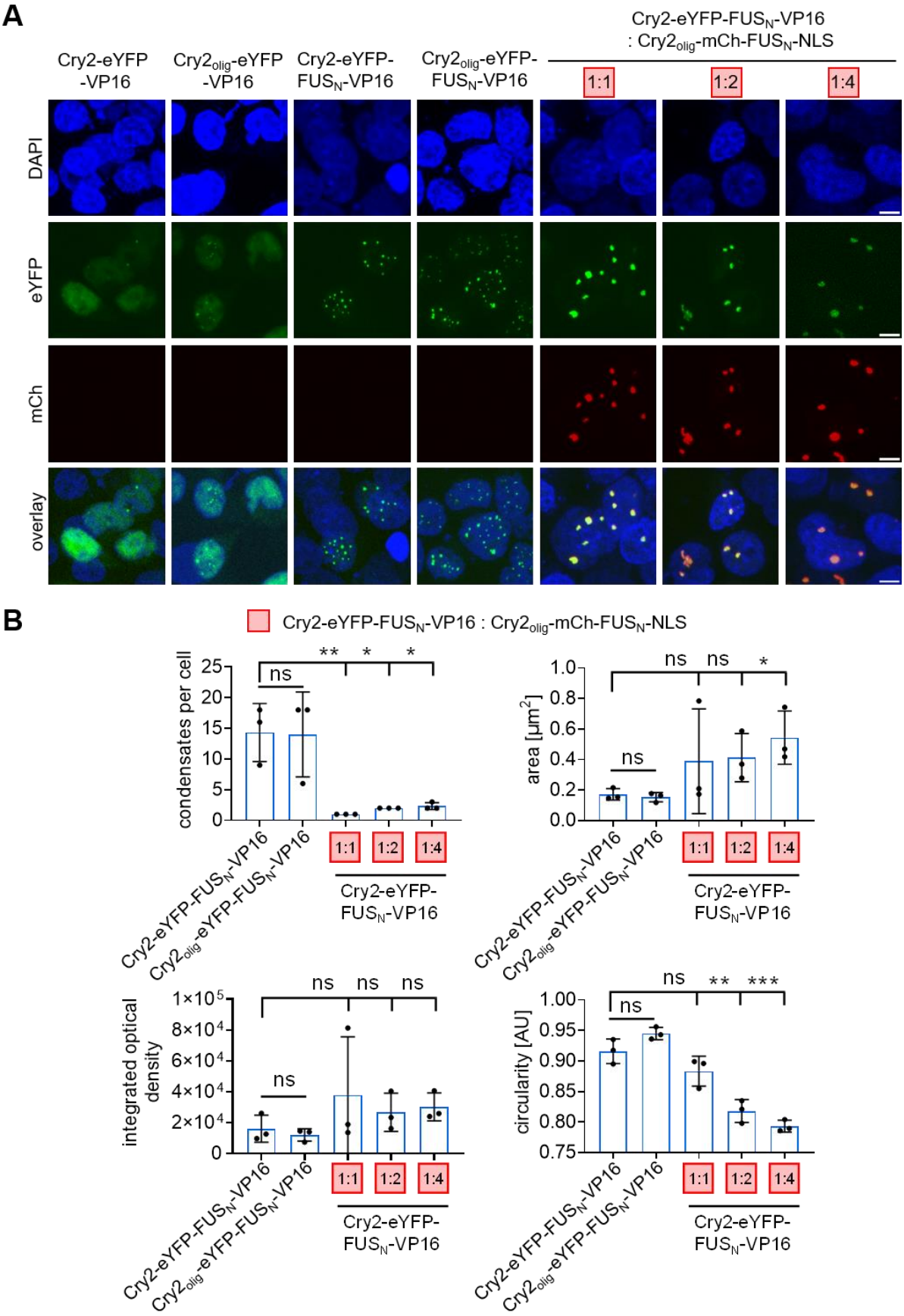
A
Cry2-eYFP -VP16
Cry2olig-eYFP -VP16
Cry2-eYFP-FUSN-VP16
Cry2olig-eYFP-FUSN-VP16
Cry2-eYFP-FUSN-VP16 : Cry2olig-mCh-FUSN-NLS
1:1
1:2
1:4
DAPI
eYFP
mCh
overlay
B
Cry2-eYFP-FUSN-VP16 : Cry2olig-mCh-FUSN-NLS
condensates per cell
area [µm2]
integrated optical density
circularity [AU]
ns
*
**
***
Cry2-eYFP-FUSN-VP16
Cry2olig-eYFP-FUSN-VP16
Cry2-eYFP-FUSN-VP16

Figure 2. Microscopical characterization of the transcription factor condensates. (**A**) Microscopy images of the condensates. HEK-293T cells were transfected with the indicated construct combinations together with a $tetO_4$-based SEAP reporter (numbers in red boxes indicate the ratios of Cry2-eYFP-FUS_N-VP16 to $Cry2_{olig}$-mCh-FUS_N-NLS constructs). 8 h post transfection, cells were illuminated with blue light for 72 h (2.5 µmol m^{-2} s^{-1}) and afterwards analyzed by microscopy. Representative microscopy images are shown; scale bar = 5 µm. (**B**) Quantitative analysis of the transcription factor condensates (only condensate forming conditions, panels 3-5). Number of condensates per cell, condensate area, integrated optical density (with regard to eYFP fluorescence), and circularity were determined. Single data points are the median of the population of one replicate, the bar represents the mean of N = 3 replicates. At least 215 cells or 1619 condensates were analyzed per condition. Pairwise comparisons were performed using a Student's t.test (* = $P < 0.05$; ** = $P < 0.01$; *** = $P < 0.001$).

2.2. Altered material properties of transcription factor condensates affect gene expression levels

To evaluate the effects of transcription factor condensates with different material properties on reporter gene expression, we analyzed transcription activity from a TetR-responsive promoter driving the expression of a secreted alkaline phosphatase (SEAP) as a reporter. We first analyzed whether the condensates co-localized with the target promoter. To this end, we used an engineered U2-OS cell line that contains 256 repeats of the lacO operator in direct proximity to a $tetO_{96}$-responsive promoter. We stained the lacO repeats by expressing the lacO-specific binding protein LacI fused to the blue-fluorescent protein (LacI-BFP). Upon co-expression of Cry2-eYFP-FUS_N-VP16 and $Cry2_{olig}$-mCh-FUS_N-NLS in the presence of the DNA-binding domain CIBN-TetR, we observed colocalization of all three fluorophores, indicating that the transcription factor condensates were indeed localized at the promoter region (Fig. 3A). Upon omission of the DNA-binding domain CIBN-TetR, no colocalization of eYFP and mCh with the BFP-stained promoter region was observed (Fig. S2A).

When analyzing the effect of transcription factor condensates on gene expression, potential differences in the expression levels of the different constructs must be considered. To ensure that the observed effects do not derive from differential transcription factor expression levels, we quantified the expression levels of our eYFP tagged transcription factors *via* flow cytometry. The observed eYFP levels are comparable between the conditions (see Fig. S2B for eYFP expression levels). We further normalized the reporter gene activity to the FACS-determined amount of transcription factor, similar to a previous study[10]. In agreement with previous reports, Cry2-eYFP-FUS_N-VP16 yielded a 3- to 4-fold increase in reporter gene expression compared to the control lacking the IDR and showing no condensate formation (Cry2-eYFP-VP16). Non-condensate-forming $Cry2_{olig}$-eYFP-VP16 showed 1.6-fold higher gene expression activities compared to Cry2-eYFP-VP16, likely due to increased clustering and therefore increased

VP16 recruitment. $Cry2_{olig}$-eYFP-FUS_N-VP16 showed a 1.5-fold increase in comparison to the non-condensate-forming, FUS_N-devoid $Cry2_{olig}$-eYFP-VP16 construct. Interestingly, with increasing amounts of $Cry2_{olig}$-mCh-FUS_N-NLS, blue-light-induced reporter expression was decreased stepwise, approximately to background levels (Fig. 3B), although the amount of activation domains (as judged from eYFP fluorescence, Fig. 2B) was increased. This finding suggests that otherwise transcription-activating factors attenuate transcription upon forming condensates with low mobile fractions.

To analyze whether the mechanism of attenuating the activating function of transcription factors by formation of low-mobility condensates is also functional in vivo, we transferred the system to mice. To this end, we first designed genetically more compact versions of the vector system to increase gene transfer efficiency in mice. We placed CIBN-TetR and Cry2-eYFP-FUS_N-VP16 on a single plasmid, either separated by posttranslational cleavage sites (T2A or a combination of T2A and P2A) or under the control of two CMV promoters in either a consecutive or bidirectional configuration (Fig. S3A). We tested the constructs using a SEAP reporter under the control of a TetR-responsive promoter and chose the bidirectional configuration, as it showed the highest dark-to-blue-light fold-induction, for all subsequent experiments (Fig. S3B). We delivered the bidirectional CIBN-TetR/Cry2-eYFP-FUS_N-VP16 construct together with a TetR-responsive luciferase reporter and increasing amounts of the $Cry2_{olig}$-mCh-FUS_N-NLS vector into mice *via* hydrodynamic tail vein injection. The mice were either kept in the dark or subjected to external blue light for 11 h prior to quantifying luciferase production, by whole-body bioluminescence imaging. In line with cell-culture experiments, blue light illumination activated luciferase production, which was gradually attenuated in the presence of increasing amounts of $Cry2_{olig}$-mCh-FUS_N-NLS (Fig. 3C, S3C).

These results suggest that modulation of the stiffness properties of synthetic transcription factor condensates by increasing valency and IDR concentration strongly impacts gene expression levels. While rather liquid condensates exert positive effects on reporter gene expression, stiffer, more dynamically arrested condensates correlate with attenuated reporter activation in mammalian cells and in mice.

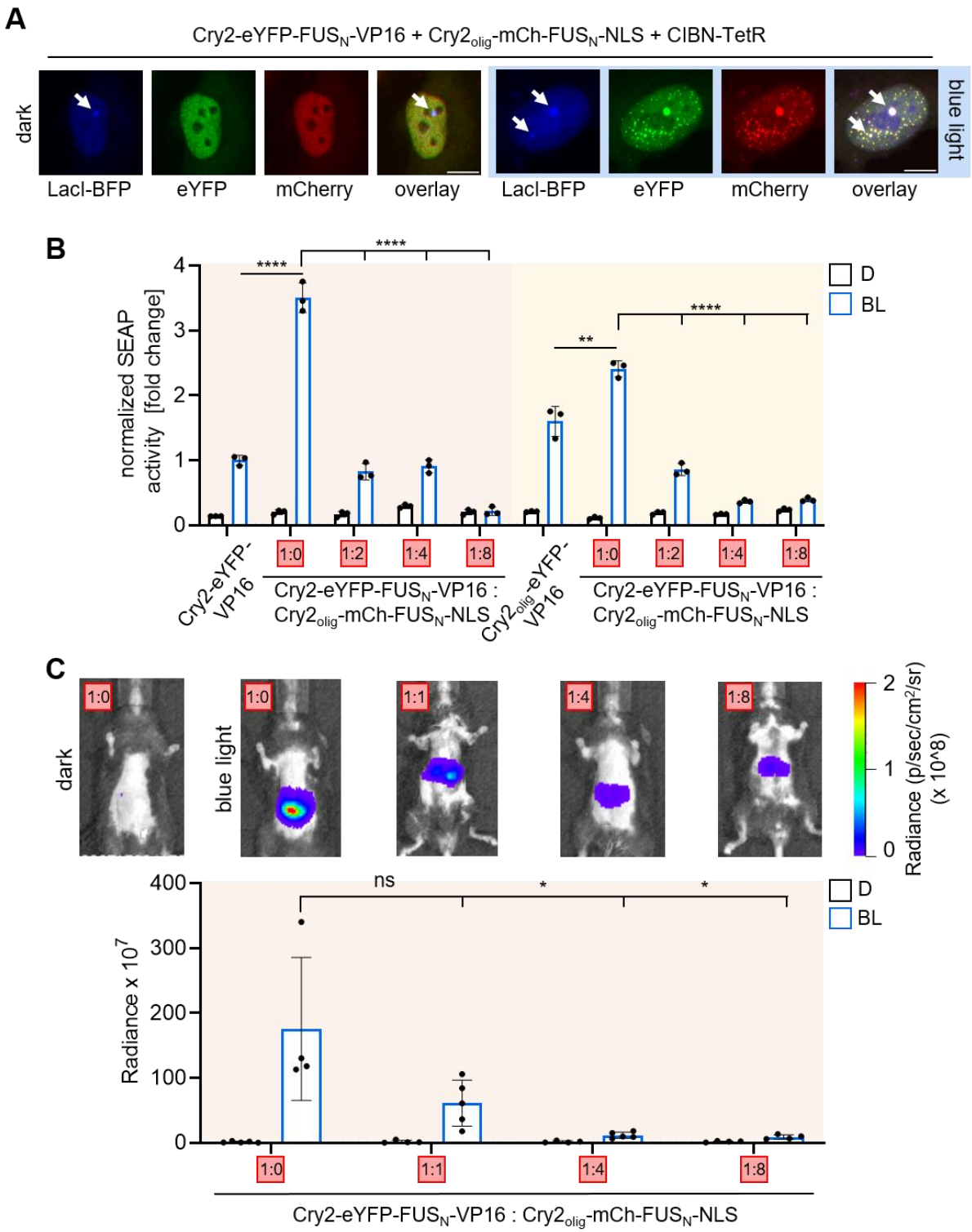

Figure 3. Influence of modified transcription factor condensate material properties on transcription. (**A**) Colocalization of transcription factor condensates with the target promoter. U2-OS cells harboring a genomic locus with 256 lacO and 96 tetO repeats were transfected with constructs for LacI-BFP, Cry2-eYFP-FUS$_N$-VP16, Cry2$_{olig}$-mCh-FUS$_N$-NLS, and CIBN-TetR. The cells were cultivated for 8 h, then illuminated for 24 h with blue light (2.5 µmol m^{-2} s^{-1}) and subjected to microscopy analysis. Scale bar = 10 µm. (**B**) Influence of transcription factor condensates on transgene expression. The indicated constructs were transfected into HEK-293T cells together with constructs for DNA-binding (CIBN-TetR) and a tetO$_4$-based SEAP reporter. The numbers in the red boxes indicate the approximate plasmid ratio of the

VP16 to mCherry-containing constructs. Cells were cultivated for 72 h in the dark (D) or under blue light (BL, 2.5 µmol m^{-2} s^{-1}) prior to quantifying SEAP and YFP production. SEAP activity values were normalized to the integrated eYFP fluorescence values of the dark samples. Data points represent the mean ± SD (N = 3). (**C**) Influence of transcription factor condensates on transgene expression in mice. Mice were hydrodynamically injected *via* the tail veins with constructs encoding CIBN-TetR and Cry2-eYFP-FUS_N-VP16 (bidirectional vector), a $tetO_7$-based firefly luciferase reporter, as well as the indicated ratios of $Cry2_{olig}$-mCh-FUS_N-NLS (red boxes, with regard to the VP16-containing construct). Eight hours after plasmid injection, the mice were exposed to blue light pulses (460 nm, 10 mW cm^{-2}, 2 min on, 2 min off, alternating) for 11 h. Subsequently, luciferin was injected intraperitoneally, and bioluminescence images were acquired. Mean bioluminescent radiance (p s^{-1} cm^{-2} sr^{-1}) ± SEM is shown (N = 4-5) together with a representative mouse image. All pairwise comparisons were performed using a Student's t.test (ns = $P > 0.05$; * = $P < 0.05$; ** = $P < 0.01$; *** = $P < 0.001$; **** = $P < 0.0001$).

2.3. Impact of condensate formation on the natural transcription factor RelA

After the characterization of our synthetic transcription factor system, we evaluated whether the same concept of increasing or decreasing transcription activation by modulating condensate material properties can be transferred to endogenous transcription factors. We chose the strong transcriptional activator RelA (p65), one of the core components of the canonical NF-κB signaling pathway.[41]

We first started with a non-optogenetic approach by fusing RelA to eYFP (eYFP-RelA) or to FUS_N and eYFP (FUS_N-eYFP-RelA). We titrated the plasmid amounts used for transfection of HEK-293T cells and observed a dose-dependent increase in the fraction of cells that showed transcription factor condensates. A low percentage of cells expressing high levels of eYFP-RelA showed formation of clusters. We then tested the capability of the two constructs to activate transcription using a dual luciferase reporter assay under the control of an NF-κB-responsive promoter.[42] In agreement with the findings for the synthetic transcription factor, condensate formation, induced by the addition of FUS_N, correlated with increased expression of the NF-κB responsive luciferase reporter (Fig. 4, S4).

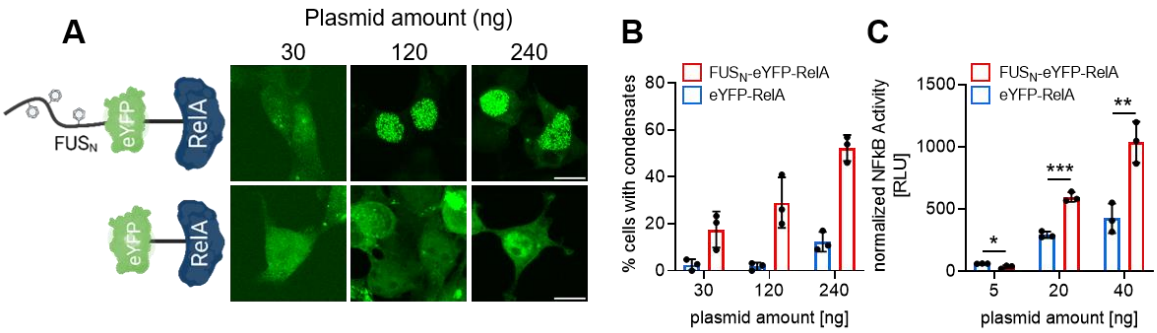

Figure 4: Influence of RelA-condensate formation on NF-κB-responsive reporter gene expression. (**A**) Condensate formation of RelA. Indicated amounts of expression constructs for RelA fused to eYFP and optionally FUS_N were transfected into HEK-293T cells together with a NF-κB-responsive firefly luciferase reporter. For internal normalization, a constitutive expression vector for renilla luciferase was co-transfected. 32 h after transfection, cells were analyzed by microscopy. Scale bar = 10 µm. Note: Minimum and maximum pixel values were adjusted differently between the panels for better visualization; quantification of the intensities is shown in the supplement. (**B**) Percentage of transfected cells that form at least 1 condensate. At least 103 cells per condition were analyzed. Mean percentages of N = 3 replicates are plotted. (**C**) Influence of RelA condensate formation on gene expression. Reporter gene expression from the experiments described in (A) was determined after 32 h of cultivation. Firefly luciferase activities were normalized to renilla luciferase activities. Values represent the mean ± SD (N = 3). *P* values were calculated using a Student's t.test: * = $P < 0.05$; ** = $P < 0.01$; *** = $P < 0.001$.

2.4. Engineering of RelA transcripton factor condensates with different material properties

Next, we evaluated the impact of light-inducible condensate stiffening on RelA activity. To this end, we fused Cry2 or $Cry2_{olig}$ to eYFP-FUS_N-RelA and then co-transfected both RelA constructs (Cry2-eYFP-FUS_N-RelA and $Cry2_{olig}$-eYFP-FUS_N-RelA) together with $Cry2_{olig}$-mCh-FUS_N-NLS into HEK-293T cells. Cells were cultured in the dark or under blue light and subsequently analyzed by microscopy. Both constructs formed condensates in the dark, which might result from a combination of RelA's intrinsic property to undergo LLPS[43] and the IDR/Cry2-containing fusion partners (Fig. 5A, B). The number of condensates per cell strongly decreased upon illumination, whereas an increase in condensate area was observed for the $Cry2_{olig}$ construct (Fig. 5B). These findings correspond to the findings from the synthetic transcription factor (Fig. 2). The eYFP integrated optical density of the condensates (reflecting the RelA amount) was similar for all conditions; only the illuminated $Cry2_{olig}$ constructs showed an increased value. For circularity, a decrease was observed for the $Cry2_{olig}$ constructs similar to the synthetic transcription factor, likely reflecting stiffer condensates (Fig. 5B). Next, we tested the activity of the different RelA condensates on transcriptional activation using the NF-κB-responsive dual luciferase reporter assay. When inducing Cry2/Cry2olig clustering by blue light illumination, a strong drop in reporter gene activity was observed for both constructs. This finding is of special interest for the combination of $Cry2_{olig}$-eYFP-FUS_N-RelA and $Cry2_{olig}$-mCh-FUS_N-NLS, where the higher levels of RelA in the condensates (see Fig. 5B, integrated optical density) after blue-light illumination might have been expected to yield higher transcriptional activation (Fig. 5C). Potential non-specific effects on reporter expression caused by the large condensates were excluded by normalizing the firefly luciferase activity with constitutively expressed renilla luciferase activity (dual luciferase assay, see above).

We conclude from these data that condensate stiffening (as induced here by the blue light-mediated multivalent interactions) counteracts the otherwise activating effect of the condensate-induced higher concentration of activation domains at the promoter site. The stiff condensates rather act as a dominant negative factor on transcriptional activation domains.

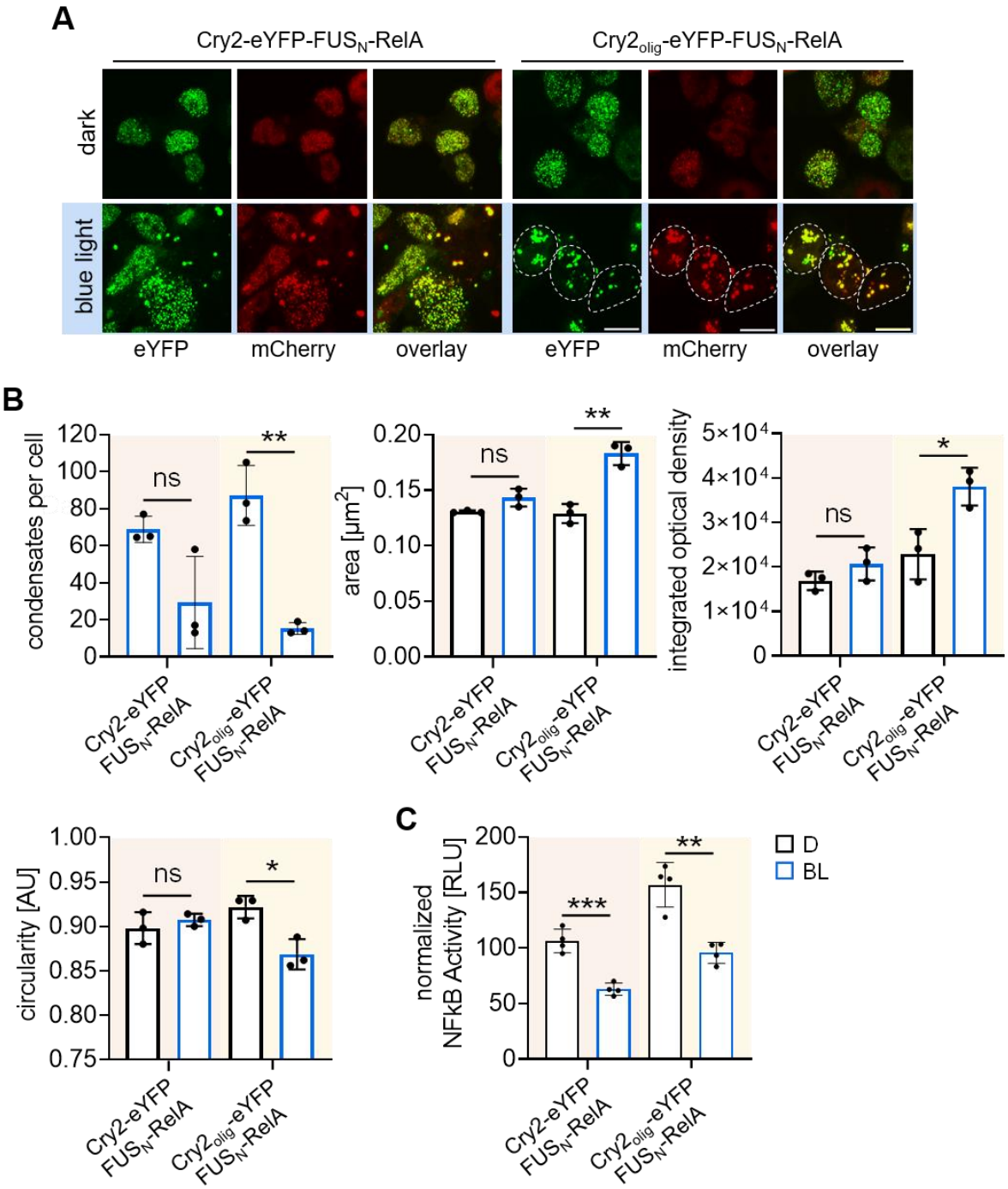

Figure 5: Optogenetic modulation of RelA-condensate material properties. (**A, B**) Optical characterization of RelA condensates. HEK-293T cells were transfected with Cry2/Cry2$_{olig}$-eYFP-FUS$_N$-RelA, Cry2$_{olig}$-mCh-FUS$_N$-NLS, an NF-κB-responsive firefly luciferase reporter, and a constitutive renilla luciferase reporter. 12 h post-transfection, cells were either kept in the dark or under illumination (5 µmol m^{-2} s^{-1}) for 40 h prior to microscopy analysis. The number of condensates per cell, condensate area, integrated optical density, and circularity were determined. At least 179 cells, or 8219 condensates, were analyzed per condition of N = 3 replicates, single data points display the median of the population of each replicate. (**C**) Influence of RelA condensates on reporter gene expression. NF-κB-responsive firefly luciferase activity from the experiment conducted as described in (**A**) was quantified. Values were normalized to constitutively expressed renilla luciferase activities. Means ± SD and single values are plotted; N = 4. All pairwise comparisons were performed using a Student's t.test (ns = $P > 0.05$; * = $P < 0.05$; ** = $P < 0.01$; *** = $P < 0.001$).

2.5. Generic downregulation of natural transcription factors activities by recruitment into stiff condensates

After demonstrating that the activity of a synthetic and a natural transcription factor can be downregulated in a dominant negative manner by genetic fusion to domains that form condensates with increased stiffness, we aimed at generalizing this approach by developing a strategy that allows easy recruitment of any protein into condensates. For recruitment, we chose an eGFP binding nanobody (NbGFP)[44] to capture arbitrary eGFP fusion proteins. We validated this concept by fusing NbGFP to either Cry2 or Cry2$_{olig}$ and further inserted mCherry (mCh, for visualization), FUS$_N$, as well as a nuclear localization sequence (NLS, Cry2/Cry2$_{olig}$-mCh-FUS$_N$-NLS-NbGFP). We then co-transfected the construct with an eGFP-RelA expression vector and analyzed condensate formation in the dark and under blue light illumination. EGFP-RelA alone showed diffusive signals both in darkness and after blue-light illumination (Fig. 6A). However, upon co-transfection with Cry2$_{olig}$-mCh-FUS$_N$-NLS and either of the NbGFP-constructs (Cry2/Cry2$_{olig}$-mCh-FUS$_N$-NLS-NbGFP), formation of large condensates was observed upon illumination. The colocalization of the mCherry and eGFP signal in the condensates further demonstrates effective recruitment of eGFP-RelA into the condensates.

When analyzing luciferase expression under the control of an NF-κB-responsive promoter, a significant decrease in luciferase activity was observed under illumination compared to the dark control, with the effect being stronger for the Cry2$_{olig}$-based construct. This finding is in line with the previous observations and demonstrates the functionality of the recruitment-based approach for condensate-mediated dominant negative regulation of otherwise activating RelA (Fig. 6B).

Next, we aimed at validating this approach with STAT3 and STAT6 transcription factors. To challenge the system, we used mutants with increased activity (STAT3$_{Y640F}$[45] and STAT6$_{V547A/T548A}$[46]) comparing them to the wild type. We co-transfected expression constructs

for $Cry2_{olig}$-mCh-FUS_N-NLS-NbGFP and $Cry2_{olig}$-mCh-FUS_N-NLS with either $STAT3_{Y640F}$-eGFP or eGFP-$STAT6_{V547A/T548A}$ vectors together with a STAT3- or STAT6-responsive luciferase reporter. The cells were further stimulated with interleukin 6 (IL-6) or interleukin 4 (IL-4) to activate STAT3 and STAT6 signaling pathways, respectively. The cells were subsequently incubated in the dark or under blue light prior to measuring luciferase activity. Upon co-transfection with the condensate-forming constructs, a 1.4- and 1.8-fold decrease in reporter output was observed for $STAT3_{Y640F}$-eGFP and eGFP-$STAT6_{V547A/T548A}$ under blue light compared to the dark control, respectively (Fig. 6C, D).

Complementarily, we performed a similar experiment this time with the transcriptional inhibitory p50 homodimer, which acts downstream of the canonical NF-κB signaling pathway and represses transcription when bound to its target promoter.[47] We transfected HEK-293T cells with the NF-κB-responsive luciferase reporter, and upon stimulation with TNF-α, high luciferase output was observed. This activity was strongly reduced upon co-transfection of an eGFP-p50 construct. Upon further co-transfection with $Cry2_{olig}$-mCh-FUS_N-NLS-NbGFP and $Cry2_{olig}$-mCh-FUS_N-NLS and illumination with blue light, a further 1.8-fold decrease in reporter output was observed compared to the dark control (Fig. 6E, S5).

From these observations, we conclude that optogenetically recruiting either activating or inhibitory transcription factors into stiff condensates can likely be used as a generally applicable principle to downregulate transcription factor activity in a light-controlled and dominant-negative manner.

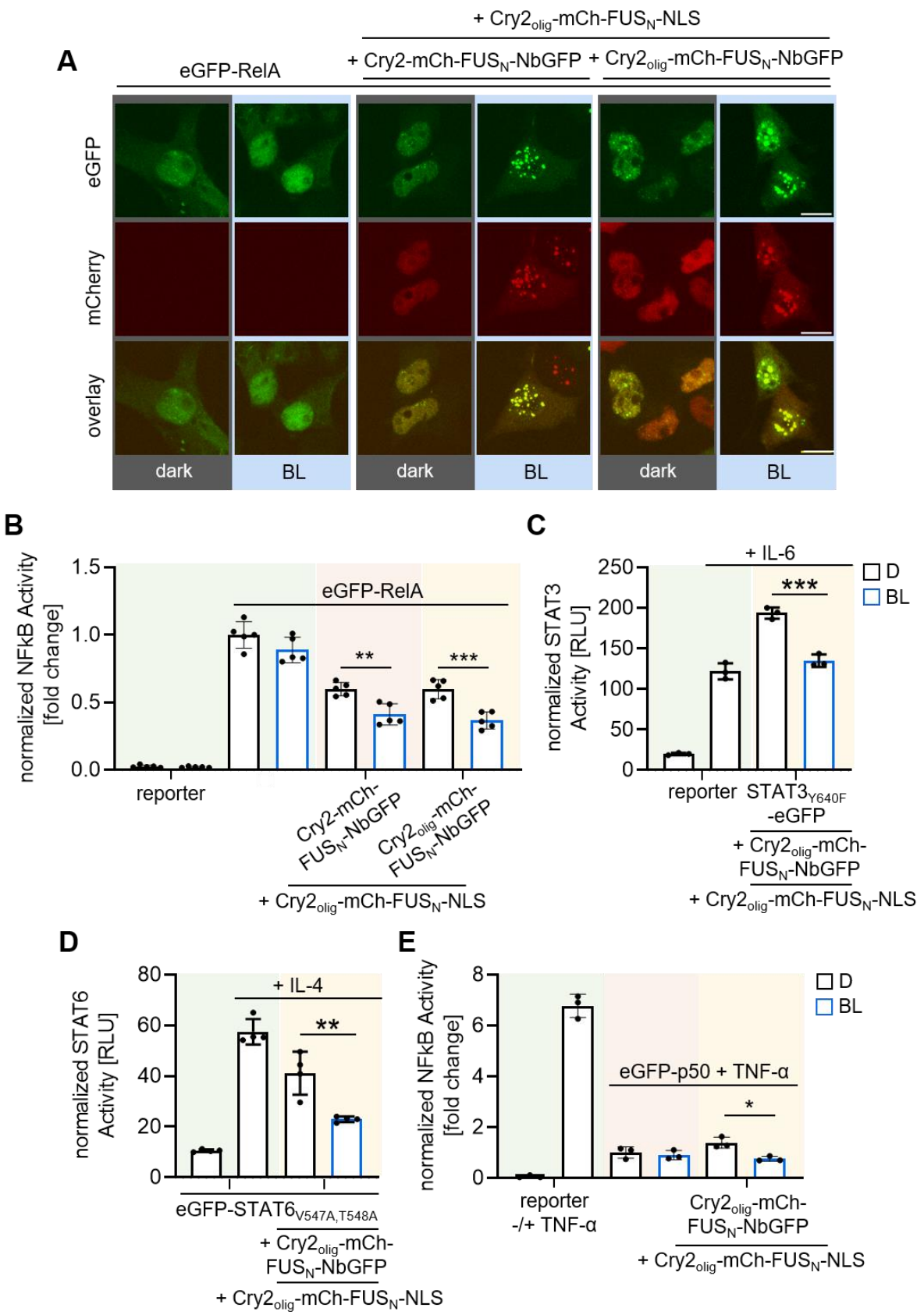
A
eGFP-RelA
+ Cry2olig-mCh-FUSN-NLS
+ Cry2-mCh-FUSN-NbGFP
+ Cry2olig-mCh-FUSN-NbGFP
eGFP
mCherry
overlay
dark
BL
B
normalized NFkB Activity [fold change]
eGFP-RelA
reporter
Cry2-mCh-FUSN-NbGFP
Cry2olig-mCh-FUSN-NbGFP
+ Cry2olig-mCh-FUSN-NLS
C
normalized STAT3 Activity [RLU]
+ IL-6
D
BL
reporter
STAT3Y640F -eGFP
+ Cry2olig-mCh-FUSN-NbGFP
+ Cry2olig-mCh-FUSN-NLS
D
normalized STAT6 Activity [RLU]
+ IL-4
eGFP-STAT6V547A,T548A
+ Cry2olig-mCh-FUSN-NbGFP
+ Cry2olig-mCh-FUSN-NLS
E
normalized NFkB Activity [fold change]
eGFP-p50 + TNF-α
reporter -/+ TNF-α
Cry2olig-mCh-FUSN-NbGFP
+ Cry2olig-mCh-FUSN-NLS

Figure 6. Generic recruitment of different transcription factors into transcription-regulating condensates. (**A**) Nanobody-mediated recruitment of RelA into condensates. HEK-293T cells were transfected with the indicated expression vectors: an NF-κB-responsive firefly luciferase expression vector as well as a constitutive renilla luciferase construct. 8 h after transfection, cells were kept in the dark (D) or under blue light (BL) illumination (5 µmol m^{-2} s^{-1}) for 24 h prior to microscopy analysis. Scale bar = 10 µm. (**B**) Impact of RelA recruitment into condensates on NF-κB-responsive gene expression. Cells were transfected as described in (**A**), and firefly luciferase activity was measured. Values were normalized to renilla luciferase activities. Means ± SD and single values are plotted; values are displayed as fold changes to eGFP-RelA (dark condition). (**C, D**) Impact of $STAT3_{Y640F}$ / $STAT6_{V547A,T548A}$ recruitment into condensates on STAT3/6-responsive gene expression. The experiment was performed as described in (**A**), except that eGFP-RelA was exchanged by eGFP-$STAT3_{Y640F}$ (**D**) or $STAT6_{V547A,T548A}$ (**E**). Cells were stimulated with 5 ng/mL IL-6 or 10 ng/mL IL-4 for $STAT3_{Y640F}$ and $STAT6_{V547A,T548A}$ experiments, respectively. (**E**) Impact of p50 recruitment into condensates on NF-κB-responsive gene expression. The experiment was performed as described in (**A**), except that eGFP-RelA was exchanged by eGFP-p50. The cells were further stimulated with 5 ng/mL TNF-α, 8 h after transfection. Data is displayed as fold change to eGFP-p50 (dark condition). N = 3-5, pairwise comparisons were performed using a Student's t.test (* = $P < 0.05$; ** = $P < 0.01$; *** = $P < 0.001$).

2.6. Light-controlled downregulation of endogenous promoters by stiff condensate formation

While all experiments above were performed with synthetic reporters as readout, we finally investigated whether the same effect can be observed for endogenous, NF-κB-responsive promoters. For this aim, we co-transfected HEK-293T cells with eGFP-RelA, $Cry2_{olig}$-mCh-FUS_N-NLS-NbGFP, and $Cry2_{olig}$-mCh-FUS_N-NLS, followed by incubation under blue light or in the dark and subsequent RT-qPCR-mediated analysis of expression levels of three NF-κB-target genes (*TNFAIP3*, *NFKBIA*, and *CXCL1*). Transfection of eGFP-RelA alone resulted in activation of the genes under either illumination condition. However, upon co-transfection with the condensate-inducing constructs, an up to 4.4-fold decrease in endogenous gene transcription was observed under illumination compared to the dark control. This finding further corroborates the above-described data and supports the hypothesis that optogenetically induced stiff transcription factor condensate formation at the promoter site is effective for the dominant-negative, light-inducible downregulation of synthetic and endogenous promoters (Fig. 7).

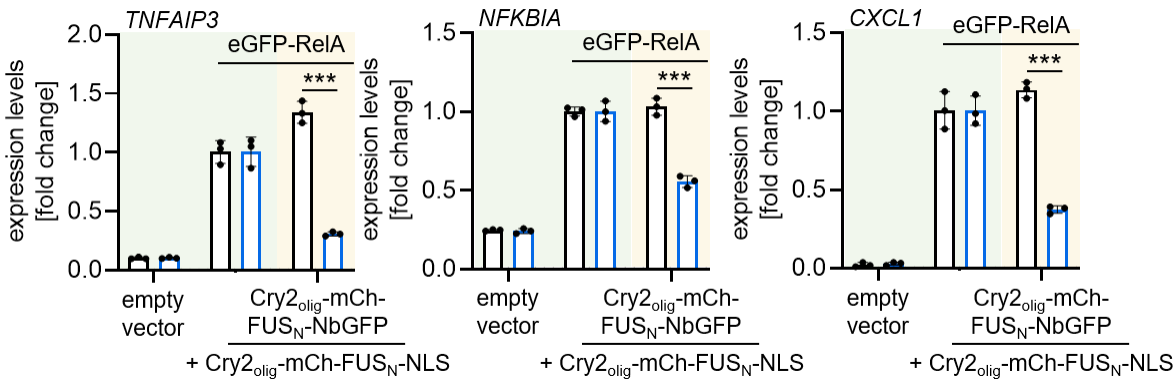

Figure 7. Impact of recruitment of RelA into condensates on endogenous gene expression. HEK-293T cells were transfected with the indicated expression vectors and an NF-κB-responsive SEAP reporter. 8 h after transfection, cells were either kept in the dark (D) or under blue light illumination (BL, 5 µmol m^{-2} s^{-1}) for 24 h prior to RNA extraction, reverse transcription, and qPCR analysis. Data was normalized to the housekeeping gene GUS. Mean $2^{\wedge -\Delta\Delta Ct}$ values ± SD are plotted as fold changes to the respective eGFP-RelA-only conditions, N = 3. *P* values were calculated using a Student's t.test on the ΔΔCt values (*** = P < 0.001).

3. Conclusion

Recent gene activation models suggest important roles for phase separation in the control of gene expression.[21,48] The IDRs of cofactors, transcription factors, or polymerase II mediate phase separation, and thereby, effective recruitment and concentration of cofactors and activators into transcriptional condensates.[49–51] Furthermore, condensates are capable of reconfiguring chromatin interactions to access enhancer regions through DNA looping, enabling long-range communication.[52,53] However, the functional impact of transcriptional condensates on gene expression levels remained inconclusive. Some groups reported positive effects[9,10,26] likely due to a higher concentration of transactivation domains at promoter regions[27] or increased recruitment of activating cofactors[51]. Other groups reported no additional effect in comparison to a multivalent but non-phase-separating transcription factor[28] or an optimum of IDRs at the promoter to achieve maximum expression levels, whereas higher IDR levels that led to condensate formation had negative effects.[29,54] Further studies suggested mechanisms such as the reduced capability of transcription factor IDRs to recruit mediators due to changes in their sequence,[55,56] recruitment of proteins that alter the surface tension and therefore reduce DNA binding capacity[57,58] or sequestration of transcription factors in the cytoplasm[59] to be involved in the downregulation of gene expression.

To investigate whether changing the material properties of transcription factor condensates could impact gene expression levels, we developed optogenetically inducible transcription factor condensates, characterized their material properties and morphology, and linked them to different levels of gene expression. We observed that liquid condensates have a positive effect

on gene expression in comparison to diffusive transcription factors, whereas stiffer condensates have negative effects. We linked functional properties to certain morphological hallmarks: stiffer condensates correlate with lower circularity, a larger area, and a lower number per cell. The latter two are likely the result of fusion events. Inhibition of gene expression occurs despite the increased transcription factor amounts within the condensates, as indicated by the increased fluorescent intensities of the condensates. The new data on the synthetic TetR-VP16-based droplet-transcription factor and the RelA-condensates suggest that rather liquid condensates increase gene expression levels in comparison to diffuse transcription factors, whereas stiff, more dynamically arrested condensates reverse this effect or even act as dominant negative factors by overcoming the capability of the transcription factors to activate gene expression.
Light is a powerful stimulus to modify protein interactions non-invasively,[60–62] and the incorporation of the eGFP-binding nanobody into the system enables flexible recruitment of arbitrary eGFP-tagged proteins into biomolecular condensates. The constructs can be used to probe protein behavior in different phase-separated conditions by modular modification of the condensate material properties, such as exchanging Cry2 with $Cry2_{olig}$ or adding $Cry2_{olig}$-mCh-FUS_N-NLS.

In conclusion, we present a designer approach for the modulation of the material properties of biomolecular transcription factor condensates. We link them to distinct biological outputs using the example of transcriptional activation. We believe that the rational design of biomolecular transcription factor condensates with defined properties will enable new avenues that allow for controlling and tuning of cellular processes or the implementation of new functions. The approach presented here is likely transferable to probe and control the function of other proteins and processes in different directions of fundamental and applied research.

4. Experimental Section

4.1. Cloning

All plasmids in this study were cloned *via* Gibson Assembly[63] or Aqua Cloning[64] and are described in Table S1. Mutations and short sequences, such as linkers, were inserted with oligonucleotides and PCR. For constructs that contain multiple repeats (promoter response elements and double vectors containing two CMV promoters), *E.coli* were grown at room temperature or maximum 30 °C. All NF-κB and STAT3-related reporters and templates for PCR amplification of NF-κB and STAT3 signaling proteins were a kind gift from the laboratory of Bodo Grimbacher (Institute for Immunodeficiency, Freiburg). All sequences were confirmed by Sanger sequencing.

4.2. Illumination

All optogenetic experiments in 96-well format were conducted in black clear-bottom plates (µCLEAR®, Greiner Bio-One, catalog no. 655090) and illuminated using the optoPlate-96[65] equipped with 470 nm LEDs (Würth Elektronik, MPN: 150141RB73100) that was programmed using the optoConfig-96[66]. Experiments in 24- or 6-well format were illuminated with micro-controller-regulated illumination panels containing LEDs with 460 nm (LED Engin, MPN: LZ1-10B202-0000). For live cell imaging, illumination was conducted directly at the confocal microscope using a pE-4000 LED light source (460 nm, CoolLED, Andover, UK). All samples that express photosensitive proteins were handled under dim, green, safe light to avoid un-wanted photoreceptor activation.

4.3. Cell culture and transfection

HEK-293T (DSMZ, catalog no. ACC 635) and U2OS 2-6-3[67] cells were cultivated in Dul-becco's modified Eagle's medium (DMEM, PAN Biotech, catalog no. P04-03550) completed with 10% (v/v) fetal calf serum (FCS, PAN Biotech, catalog no. P30-3602) and 1% (v/v) peni-cillin-streptomycin (PAN Biotech, catalog no. P06-07100) at 37 °C and 5% CO_2. They were passaged every 2-3 days after reaching a confluency of ≈ 80%. For experiments, cells were seeded into multi-well plates and transfected with polyethyleneimine (PEI, 1 mg/ml in H_2O, pH 7, Polyscience, catalog no. 23966-1). Therefore, DNA and PEI were prepared separately, each in half of the total volume Opti-MEM (Thermo Fisher Scientific, catalog no. 22600-134). The two approaches were mixed, immediately vortexed for 15 s, and incubated for 15 min at room temperature. DNA/PEI mixes were then applied dropwise to the cells. Cells transfected for optogenetic experiments were then kept in darkness. Exact plasmid combinations and amounts for each experiment are listed in Table S2.

4.4. Reporter assays

All reporter assays (SEAP and dual-luciferase) were performed in 96-well plates (non-optoge-netic experiments: Corning, catalog no. 3596; optogenetic experiments: µCLEAR®, Greiner Bio-One, catalog no. 655090). 15,000 cells per well in 100 µl DMEM were seeded ≈ 24 h prior to transfection. For transfection, 125 ng DNA and 0.41 µl polyethyleneimine in 20 µl Opti-MEM per well were used. For optogenetic experiments, illumination was started 8-12 h after transfection, and the assays were conducted 24-72 h after transfection, as indicated for each

experiment. For the readout, either a Synergy 4 multimode microplate reader (BioTek Instruments Inc.), an Infinite 200Pro microplate reader (Tecan Trading AG), or a SpectraMax iD5 microplate reader (Molecular Devices GmbH) was used.

For firefly/renilla dual luciferase assays, cells were lysed by addition of 100 µl lysis buffer (25 mM Tris/HCl, pH 7.8, 1% Triton X-100 (v/v), 15 mM $MgSO_4$, 4 mM ethylene glycol tetraacetic acid (EGTA), 1 mM DTT) per well. After 5 min of incubation at room temperature (RT), cells were resuspended and split into 2x 40 µl samples by transferring them into two white flat-bottom 96-well plates (Corning Incorporated, catalog no. CORN3912). The plates were spun down for 30 s at 1200 rpm to remove all bubbles. One plate was used for Firefly luciferase measurement by addition of 20 µl firefly substrate (0.47 mM luciferin in 20 mM Tricine, 2.67 mM $MgSO_4$, 0.1 mM EDTA, 33.3 mM DTT, 0.52 mM ATP, 0.27 mM Acetyl-CoA, 5 mM NaOH, 0.264 mM $MgCO_3$) per well, and the other plate was used for renilla luciferase measurement by addition of 20 µl coelenterazine (stock: 472 µM coelenterazine in methanol; diluted 1:10 in PBS directly before measurement) per well. Both plates were measured immediately after substrate addition (program: 10 s shaking, 1000 ms integration time, endpoint measurement). Firefly values were normalized with background-subtracted renilla values.

For SEAP activity measurement, the whole supernatant was transferred into a U-bottom transparent 96-well plate (Carl Roth, catalog no. 9291.1), sealed with adhesive tape, and heated at 65 °C for 30 min. Afterwards, samples were spun down for 3 min at 1250 rpm, then 80 µl supernatant was added to 100 µl 2x SEAP buffer (21% (v:v) diethanolamine, 20 mM L-homoarginine-hydrochloride, 1 mM $MgCl_2$ (pH 9.8)) in transparent flat-bottom 96-well plates (Carl Roth, catalog no. 9293.1). Directly prior to the measurement, 20 µl para-nitrophenylphosphate solution (pNPP, 120 mM) was added, and its conversion to para-nitrophenol by SEAP was measured by absorbance at 405 nm in time intervals of 1 min. SEAP activity was calculated as described previously.[68]

4.5. Flow cytometry

For comparison between different constructs in reporter assays, the expression levels of the fluorescent proteins in each construct were determined by flow cytometry. Therefore, medium was removed and cells were detached with 50 µl trypsin/EDTA solution (PAN Biotech, catalog no. P10-023500) per well. Afterwards, 150 µl PBS supplemented with 2% (v/v) FCS was added, and cells were carefully resuspended and transferred into a transparent U-bottom 96-well plate (Greiner, catalog no. 650161). Cells were kept on ice until measurement with an Attune NxT flow (Thermo Fisher Scientific). EGFP and EYFP were measured by excitation with a 488 nm

laser and detected with a 530/30 nm emission filter (BL1) and mCherry was measured with a 561 nm excitation laser and a 620/15 nm emission filter (YL2). 15,000 cells per well were analyzed at a flow rate of 200 µl/min. Analysis was performed using the FlowJo_v10™ software. Singlets were gated, and the integrated eYFP intensity was used for normalization.

4.6. Microscopy and image analysis

For microscopy of fixed samples, coverslips (Carl Roth, catalog no. YX03.2) were placed in 24-well plates (Corning, catalog no. CORN3524) and coated with 500 µl rat tail collagen I (Thermo Fisher Scientific, catalog no. A1048301) at a concentration of 50 µg/ml diluted in 25 mM acetic acid. After one hour of incubation at RT, the wells were washed three times with 500 µl PBS, and 75,000 cells per well were seeded. For transfection in 24-well format, 750 ng DNA and 2.4 µl PEI in 100 µl OptiMEM per well were used. Illumination of optogenetic experiments was started after 8 h for time periods as indicated in the figure legends. Cells were fixed by removing the medium and adding 200 µl methanol-free paraformaldehyde (PFA, Science Services, catalog no. E15714-S; 4% diluted in PBS (v/v)) under green safe light. After 15 min of incubation at RT in darkness, PFA was removed, and cells were washed twice with 500 µl PBS. For staining of the nuclei, 500 µl 0.2 µg/ml 4',6'-diamidino-2-phenylindole (DAPI, Merck, catalog no. D9542) in PBS was added for 15 min at RT, then cells were washed again twice with 500 µl PBS and mounted on microscopy slides with 8.5 µl Mowiol mounting medium (2.4 g Mowiol, 6 g glycerol, 6 ml of H_2O, and 12 ml of Tris/HCl (pH 8.5)). After the samples were dried, the edges were additionally fixed with transparent nail polish. All images and time series were acquired with a Zeiss LSM 880 laser scanning confocal microscope using a 63x Plan-Apochromat oil objective (NA 1.4) in z-stacks of 12 focal planes with a distance of 1 µm. DAPI was imaged with the 405 nm laser, eGFP and eYFP were excited with the 488 nm laser, and mCherry with the 561 nm laser.

For quantitative image analysis, at least 2 images of 3 replicates were acquired. Z-stacks were reduced to two-dimensional maximum intensity projections. The percentage of cells that form droplets was determined by first segmenting and counting the transfected cells and then manually counting the cells with droplets. For analysis of the droplet properties, nuclei and droplets were segmented and analyzed using custom-written macros for ImageJ 2.3.0/1.53q including the Biovoxxel Toolbox v2.6.0.[69] A threshold for minimum 1 droplet per cell with a size of at least 0.017 μm^2 (7 pixel) was set. For droplet intensity, the RawIndDen (sum of all pixel values of the droplet) was used. All macro outputs were manually double-checked. If not stated otherwise, minimum, and maximum pixel values of a channel were adjusted equally for all samples

of an experiment. In overlay images, intensities may be adjusted differently for better visualization of all channels.

FRAP measurements were conducted in 35 mm glass bottom dishes (µ-Dish 35 mm, high, Ibidi cat. No. 81156) using a Tokai Hit stage top incubator under continuous illumination with the pE-4000 CoolLED (460 nm, 5 µmol m^{-2} s^{-1}). Time series of at least 300 s were acquired as z-stacks of nine focal planes with a distance of 600 nm, an interval of every 5 s and the zoom factor six. Four eYFP droplets were selected simultaneously with regions of interest (ROI) of ≈ 0.8 µm diameter and bleached after the first z-stack was acquired, using 100% laser power of the 488 nm laser. For analysis, droplets were manually tracked with a circular mask of constant diameter in the x, y and z directions for 300 seconds. Afterwards, background signals were subtracted, and droplet recovery was corrected for photobleaching by normalization with the linear regression of the average fluorescence signal decrease of the nuclei. Values were normalized to the intensity before and directly after bleaching. Mobile fractions were calculated by fitting the recovery curves to an exponential plateau equation using GraphPad Prism 9.2.0.

4.7. Reverse transcription quantitative PCR (RT-qPCR)

For RNA extractions, 600,000 cells/well were seeded onto 6-well plates (Corning, catalog no. CORN3516) and 24 h later transfected with 600 µl transfection mix containing 3.750 µg total DNA and 12.375 µl PEI per well. Blue-light illumination (460 nm, 5 µmol m^{-2} s^{-1}) was started 8 h after transfection. Cells were harvested 24 h later using 1 mL TriFast™ (VWR, cat. no. 30-2010) per well. Total RNA was extracted according to the manufacturer's protocol. RNA integrity was verified on an agarose gel, and concentrations, 260/280 and 230/280 ratios were determined with a nanodrop 1000 (Thermo Fisher Scientific). Reverse transcription was performed using the High Capacity Kit (Applied Biosystems™, cat. no. 4368814) according to the manufacturer's protocol using 2 µg RNA. The resulting cDNA was diluted 1:20 and used for qPCR. The primers for the three NF-κB target genes were selected from literature (NFKBIA, oAF469: 5'- ATGTCAATGCTCAGGAGCCC-3' and oAF470: 5'-GACATCAGCCCCACACTTCA-3';[70] TNFAIP3, oAF467: 5'-CGTCCAGGTTCCAGAACACCATTC-3' and oAF468: 5'- TGCGCTGGCTCGATCTCAG-TTG-3';[71] CXCL1, oAF471: 5'-AACCGAAGTCATAGCCACAC-3' and oAF472: 5'-GTT-GGATTTGTCACTGTTCAGC-3'[72]) and GUS was used as housekeeping gene (oMH703/oAF481, 5'-CGTCCCACCTAGAATCTGCT-3' and oMH702/oAF482, 5'-TTGCTCACAAAGGTCACAGG-3'). qPCRs were conducted with a CFX384 Touch Real-Time PCR Detection System (BioRad) in 10 µl approaches with the PowerTrack™ SYBR

Green Mastermix (Applied Biosystems™, cat. no. A46110) according to the manufacturer's protocol (fast cycling mode with default dissociation step). ΔΔCt analysis was performed with the means of three technical replicates and the housekeeping gene GUS. Data is displayed as fold-changes to the eGFP-RelA containing control. Single data points display the biological replicates.

4.8. Mouse experiments

All the animals were obtained from the ECNU Laboratory Animal Centre, kept on a standard alternating 12-h light/12-h dark cycle, and were given a normal chow diet [6% fat and 18% protein (wt/wt)] and water. Wild-type C57BL/6 mice (6-week-old, male) were randomly divided into four groups. The mice were hydrodynamically injected in their tail vein with a total amount of 330 µg in 2 mL (10% of the body weight in grams) of Ringer's solution (147 mM NaCl, 4 mM KCl and 1.13 mM $CaCl_2$) within 3-5 s. Plasmid combinations are described in Table S2. Eight hours after injection, the mice were exposed to blue light pulses (460 nm, 10 mW cm^{-2}, 2 min on, 2 min off alternating; Shenzhen Kiwi Lighting Co. Ltd.) for 11 h. The control mice were kept in the dark. For in vivo bioluminescence imaging, each mouse was intraperitoneally injected with luciferin substrate solution (150 mg/kg; luc001, Shanghai Sciencelight Biology Science & Technology) under ether anesthesia. Five minutes after luciferin injection, bioluminescence images of the mice were acquired using the IVIS Lumina II in vivo imaging system (Perkin Elmer, USA). Radiance (p sec^{-1} cm^{-2} sr^{-1}) values were calculated for the region of interest using the Living Image® 4.3.1 software.

4.9. Software

All analyses were performed with Microsoft Excel 2016 and GraphPad Prism 9.2.0. FACS data was analyzed with FlowJo_v10™, and image analysis was done with ImageJ 2.3.0/1.53q including the Biovoxxel Toolbox v2.6.0[69]. The bioluminescent mouse images were analyzed with the Living Image® 4.3.1 software. All schemes were created with BioRender.com.

Ethics

The experiments involving animals were approved by the East China Normal University (ECNU) Animal Care and Use Committee and in direct accordance with the Ministry of Science and Technology of the People's Republic of China on Animal Care guidelines. The protocol (protocol ID: m20221109) was approved by the ECNU Animal Care and Use Committee. All animals were euthanized after the termination of the experiments.

Funding

This work was supported by the German Research Foundation (Deutsche Forschungsgemeinschaft, DFG) under Germany's Excellence Strategy – CIBSS, EXC-2189, Project ID: 390939984 and under the Excellence Initiative of the German Federal and State Governments – BIOSS, EXC-294 and SGBM, GSC-4, and in part by the Ministry for Science, Research and Arts of the State of Baden-Württemberg. This work was also partially supported by the National Natural Science Foundation of China (NSFC: no.32250010, no.32261160373, no.31971346) to H.Y.

Author contributions

A.A.M.F., D.K., M.M.G., J.G. and J.G. have performed experimental work. A.A.M.F. and W.W. analyzed the results and wrote the manuscript. M.F. and B.G. were valuable advisors. H.Y. and W.W. supervised the work. All authors edited and approved the manuscript.

Competing interests

The authors declare that they have no competing interests.

Data and materials availability

All data needed to evaluate the conclusions in the paper is present in the paper and/or Supplementary Materials. Raw data (images, FACS data, SEAP and Luciferase measurements), plasmids and detailed plasmid maps are available from the authors upon request.

Acknowledgements

We are very grateful to M. Klenzendorf and D. Gaspar for excellent technical assistance and to L. Qiao for excellent assistance in the animal work. We thank all members of the Weber laboratory for their helpful comments, especially N. Schneider, M. Hörner and O. Thomas for valuable advices. We would like to thank the Faculty of Biology technical workshop for the construction of the illumination devices. We acknowledge the excellent scientific and technical assistance of the Signalling Factory Core Facility staff of the Albert-Ludwigs-University Freiburg for help on flow cytometry, especially P. Salavei and N. Gensch. We acknowledge the staff of the Life Imaging Center (LIC) in the Center for Biological Systems Analysis (ZBSA)

of the Albert-Ludwigs-University Freiburg for their help with microscopy resources, and their excellent support in microscopy setup and image acquisition.

Received: ((will be filled in by the editorial staff))
Revised: ((will be filled in by the editorial staff))
Published online: ((will be filled in by the editorial staff))

References

[1] S. F. Banani, H. O. Lee, A. A. Hyman, M. K. Rosen, *Nat. Rev. Mol. Cell Biol.* **2017**, *18*, 285.

[2] A. S. Lyon, W. B. Peeples, M. K. Rosen, *Nat. Rev. Mol. Cell Biol.* **2021**, *22*, 215.

[3] Y. Dai, L. You, A. Chilkoti, *Nat. Rev. Bioeng.* **2023**, *1*, 466.

[4] H. Ruan, C. D. Reinkemeier, A. Obarska-kosinska, M. Siggel, **2023**, *617*, 162.

[5] H. Guo, J. C. Ryan, X. Song, A. Mallet, M. Zhang, V. Pabst, A. L. Decrulle, P. Ejsmont, E. H. Wintermute, A. B. Lindner, *Cell* **2022**, *185*, 3823.

[6] E. M. Zhao, N. Suek, M. Z. Wilson, E. Dine, N. L. Pannucci, Z. Gitai, J. L. Avalos, J. E. Toettcher, *Nat. Chem. Biol.* **2019**, *15*, 589.

[7] Y. Shin, Y. C. Chang, D. S. W. Lee, J. Berry, D. W. Sanders, P. Ronceray, N. S. Wingreen, M. Haataja, C. P. Brangwynne, *Cell* **2018**, *175*, 1481.

[8] J. M. Eeftens, M. Kapoor, D. Michieletto, C. P. Brangwynne, *Nat. Commun.* **2021**, *12*, 5888.

[9] M.-T. Wei, Y.-C. Chang, S. F. Shimobayashi, Y. Shin, A. R. Strom, C. P. Brangwynne, *Nat. Cell Biol.* **2020**, *22*, 1187.

[10] N. Schneider, F. G. Wieland, D. Kong, A. A. M. Fischer, M. Hörner, J. Timmer, H. Ye, W. Weber, *Sci. Adv.* **2021**, *7*, eabd3568.

[11] M. Kato, T. W. Han, S. Xie, K. Shi, X. Du, L. C. Wu, H. Mirzaei, E. J. Goldsmith, J. Longgood, J. Pei, N. V. Grishin, D. E. Frantz, J. W. Schneider, S. Chen, L. Li, M. R. Sawaya, D. Eisenberg, R. Tycko, S. L. McKnight, *Cell* **2012**, *149*, 753.

[12] T. W. Han, M. Kato, S. Xie, L. C. Wu, H. Mirzaei, J. Pei, M. Chen, Y. Xie, J. Allen, G. Xiao, S. L. McKnight, *Cell* **2012**, *149*, 768.

[13] A. Molliex, J. Temirov, J. Lee, M. Coughlin, A. P. Kanagaraj, H. J. Kim, T. Mittag, J. P. Taylor, *Cell* **2015**, *163*, 123.

[14] A. Patel, H. O. Lee, L. Jawerth, S. Maharana, M. Jahnel, M. Y. Hein, S. Stoynov, J.

Mahamid, S. Saha, T. M. Franzmann, A. Pozniakovski, I. Poser, N. Maghelli, L. A. Royer, M. Weigert, E. W. Myers, S. Grill, D. Drechsel, A. A. Hyman, S. Alberti, *Cell* **2015**, *162*, 1066.

[15] S. Qamar, G. Wang, S. J. Randle, T. Knowles, M. Vendruscolo, P. S. George-hyslop, S. Qamar, G. Wang, S. J. Randle, F. S. Ruggeri, J. A. Varela, **2018**, 720.

[16] J. Wang, J. M. Choi, A. S. Holehouse, H. O. Lee, X. Zhang, M. Jahnel, S. Maharana, R. Lemaitre, A. Pozniakovsky, D. Drechsel, I. Poser, R. V. Pappu, S. Alberti, A. A. Hyman, *Cell* **2018**, *174*, 688.

[17] W. T. Snead, A. S. Gladfelter, *Mol. Cell* **2019**, *76*, 295.

[18] B. Tsang, I. Pritišanac, S. W. Scherer, A. M. Moses, J. D. Forman-Kay, *Cell* **2020**, *183*, 1742.

[19] Y. Shin, J. Berry, N. Pannucci, M. P. Haataja, J. E. Toettcher, C. P. Brangwynne, *Cell* **2017**, *168*, 159.

[20] D. Bracha, M. T. Walls, M.-T. Wei, L. Zhu, M. Kurian, J. L. Avalos, J. E. Toettcher, C. P. Brangwynne, *Cell* **2018**, *175*, 1467.

[21] D. Hnisz, K. Shrinivas, R. A. Young, A. K. Chakraborty, P. A. Sharp, *Cell* **2017**, *169*, 13.

[22] S. Chong, C. Dugast-Darzacq, Z. Liu, P. Dong, G. M. Dailey, C. Cattoglio, A. Heckert, S. Banala, L. Lavis, X. Darzacq, R. Tjian, *Science (80-.).* **2018**, *361*, eaar2555.

[23] A. Boija, I. A. Klein, B. R. Sabari, A. Dall'Agnese, E. L. Coffey, A. V Zamudio, C. H. Li, K. Shrinivas, J. C. Manteiga, N. M. Hannett, B. J. Abraham, L. K. Afeyan, Y. E. Guo, J. K. Rimel, C. B. Fant, J. Schuijers, T. I. Lee, D. J. Taatjes, R. A. Young, *Cell* **2018**, *175*, 1842.

[24] J. E. Henninger, O. Oksuz, K. Shrinivas, I. Sagi, G. LeRoy, M. M. Zheng, J. O. Andrews, A. V. Zamudio, C. Lazaris, N. M. Hannett, T. I. Lee, P. A. Sharp, I. I. Cissé, A. K. Chakraborty, R. A. Young, *Cell* **2021**, *184*, 207.

[25] T. Hirose, K. Ninomiya, S. Nakagawa, T. Yamazaki, *Nat. Rev. Mol. Cell Biol.* **2023**, *24*, 288.

[26] J. Wu, B. Chen, Y. Liu, L. Ma, W. Huang, Y. Lin, *Nat. Commun.* **2022**, 1.

[27] D. A. Garcia, T. A. Johnson, D. M. Presman, G. Fettweis, K. Wagh, L. Rinaldi, D. A. Stavreva, V. Paakinaho, R. A. M. Jensen, S. Mandrup, A. Upadhyaya, G. L. Hager, *Mol. Cell* **2021**, *81*, 1484.

[28] J. Trojanowski, L. Frank, A. Rademacher, N. Mücke, P. Grigaitis, K. Rippe, *Mol. Cell* **2022**, *82*, 1878.

[29] S. Chong, T. G. W. Graham, C. Dugast-Darzacq, G. M. Dailey, X. Darzacq, R. Tjian, *Mol. Cell* **2022**, *82*, 2084.

[30] B. Shi, W. Li, Y. Song, Z. Wang, R. Ju, A. Ulman, J. Hu, F. Palomba, Y. Zhao, J. P. Le, W. Jarrard, D. Dimoff, *Nature* **2021**, *597*, DOI 10.1038/s41586-021-03903-7.

[31] W. Li, J. Hu, B. Shi, F. Palomba, M. A. Digman, E. Gratton, *Nat. Cell Biol.* **2020**, *22*, DOI 10.1038/s41556-020-0550-8.

[32] Z. Wang, J. Lou, H. Zhang, *J. Biol. Chem.* **2022**, *298*, 101782.

[33] C. Guo, Z. Luo, C. Lin, *Biochemistry* **2022**, *61*, 2456.

[34] S. J. Nair, L. Yang, D. Meluzzi, S. Oh, F. Yang, M. J. Friedman, S. Wang, T. Suter, I. Alshareedah, A. Gamliel, Q. Ma, J. Zhang, Y. Hu, Y. Tan, K. A. Ohgi, R. S. Jayani, P. R. Banerjee, A. K. Aggarwal, M. G. Rosenfeld, *Nat. Struct. Mol. Biol.* **2019**, *26*, 193.

[35] S. Alberti, A. A. Hyman, *Nat. Rev. Mol. Cell Biol.* **2021**, 1.

[36] Z. Wang, D. Chen, D. Guan, X. Liang, J. Xue, H. Zhao, G. Song, J. Lou, Y. He, **2022**, *221*.

[37] A. Rademacher, F. Erdel, J. Trojanowski, S. Schumacher, K. Rippe, *J. Cell Sci.* **2017**, *130*, 4213.

[38] A. Taslimi, J. D. Vrana, D. Chen, S. Borinskaya, B. J. Mayer, M. J. Kennedy, C. L. Tucker, *Nat. Commun.* **2014**, *5*, 4925.

[39] Y. Gao, X. Li, P. Li, **2022**, *18*, 1307.

[40] S. Alberti, A. Gladfelter, T. Mittag, *Cell* **2019**, *176*, 419.

[41] A. Oeckinghaus, S. Ghosh, *Cold Spring Harb. Perspect. Biol.* **2009**, *1*, a000034.

[42] P. Schneider, L. Willen, C. R. Smulski, *Tools and Techniques to Study Ligand-Receptor Interactions and Receptor Activation by TNF Superfamily Members*, Elsevier Inc., **2014**.

[43] J. N. Wibisana, T. Inaba, H. Shinohara, N. Yumoto, T. Hayashi, M. Umeda, M. Ebisawa, I. Nikaido, Y. Sako, M. Okada, *PLoS Genet.* **2022**, *18*, 1.

[44] A. Kirchhofer, J. Helma, K. Schmidthals, C. Frauer, S. Cui, A. Karcher, M. Pellis, S. Muyldermans, C. S. Casas-Delucchi, C. Cardoso, H. Leonhardt, K.-P. Hopfner, U. Rothbauer, *Nat. Struct. Mol. Biol.* **2009**, *17*, 133.

[45] R. Mori, J. Wauman, L. Icardi, J. Van Der Heyden, L. De Cauwer, F. Peelman, K. De Bosscher, J. Tavernier, *Sci. Rep.* **2017**, *7*, 1.

[46] C. Daniel, A. Salvekar, U. Schindler, *J. Biol. Chem.* **2000**, *275*, 14255.

[47] M. S. Hayden, S. Ghosh, *Genes Dev.* **2004**, *18*, 2195.

[48] P. Bhat, D. Honson, M. Guttman, *Nat. Rev. Mol. Cell Biol. 2021 2210* **2021**, *22*, 653.

[49] B. R. Sabari, B. R. Sabari, A. D. Agnese, A. Boija, I. A. Klein, E. L. Coffey, B. J. Abraham, N. M. Hannett, A. V Zamudio, J. C. Manteiga, C. H. Li, Y. E. Guo, D. S. Day, J. Schuijers, E. Vasile, S. Malik, D. Hnisz, T. I. Lee, I. I. Cisse, R. G. Roeder, P. A. Sharp, A. K. Chakraborty, R. A. Young, **2018**, *3958*, 1.

[50] W. Cho, J. Spille, M. Hecht, C. Lee, C. Li, V. Grube, I. I. Cisse, **2018**, *4199*, 1.

[51] L. Ma, Z. Gao, J. Wu, B. Zhong, Y. Xie, W. Huang, Y. Lin, *Mol. Cell* **2021**, *81*, 1682.

[52] Y. J. Kim, M. L. Jr, Y. Lee, J. Jing, J. T. Sanders, G. A. Botten, L. He, J. Lyu, Y. Zhang, M. Mettlen, P. Ly, Y. Zhou, J. Xu, **2023**, 1.

[53] K. Shrinivas, B. R. Sabari, E. L. Coffey, I. A. Klein, A. Boija, A. V Zamudio, J. Schuijers, N. M. Hannett, P. A. Sharp, R. A. Young, A. K. Chakraborty, *Mol. Cell* **2019**, *75*, 549.

[54] L. Song, X. Yao, H. Li, B. Peng, A. P. Boka, Y. Liu, G. Chen, Z. Liu, K. M. Mathias, L. Xia, Q. Li, M. Mir, Y. Li, H. Li, L. Wan, *Mol. Cell* **2022**, *82*, 4080.

[55] S. Basu, S. D. Mackowiak, H. Niskanen, D. Knezevic, V. Asimi, S. Grosswendt, H. Geertsema, S. Ali, I. Jerković, H. Ewers, S. Mundlos, A. Meissner, D. M. Ibrahim, D. Hnisz, *Cell* **2020**, *181*, 1062.

[56] W. Li, H. Jiang, *J. Mol. Biol.* **2022**, *434*, 167151.

[57] Z. Wang, C. Yang, D. Guan, J. Li, H. Zhang, *Dev. Cell* **2023**, *58*, 919.

[58] M. Takla, S. Keshri, D. C. Rubinsztein, *EMBO Rep.* **2023**, 1.

[59] F. Jobe, J. Simpson, P. Hawes, E. Guzman, D. Bailey, *J. Virol.* **2020**, *94*, e01380.

[60] A. A. M. Fischer, M. M. Kramer, G. Radziwill, W. Weber, *Curr. Opin. Chem. Biol.* **2022**, *70*, 102196.

[61] K. Kolar, C. Knobloch, H. Stork, M. Žnidarič, W. Weber, *ACS Synth. Biol.* **2018**, *7*, 1825.

[62] K. Kolar, W. Weber, *Curr. Opin. Biotechnol.* **2017**, *47*, 112.

[63] D. G. Gibson, L. Young, R. Y. Chuang, J. C. Venter, C. A. Hutchison, H. O. Smith, *Nat. Methods* **2009**, *6*, 343.

[64] H. M. Beyer, P. Gonschorek, S. L. Samodelov, M. Meier, W. Weber, M. D. Zurbriggen, *PLoS One* **2015**, *10*, e0137652.

[65] L. J. Bugaj, W. A. Lim, *Nat. Protoc. 2019 147* **2019**, *14*, 2205.

[66] O. S. Thomas, M. Hörner, W. Weber, *Nat. Protoc.* **2020**, *15*, 2785.

[67] S. M. Janicki, S. E. Salghetti, W. P. Tansey, R. Sachidanandam, K. V Prasanth, D. L. Spector, T. Tsukamoto, T. Ried, Y. Shav-Tal, R. H. Singer, E. Bertrand, *Cell* **2004**, *116*, 683.

[68] S. Schlatter, M. Rimann, J. Kelm, M. Fussenegger, *Gene* **2002**, *282*, 19.

[69] J. Brocher, **2023**, DOI https://zenodo.org/record/8214743.

[70] A. Callegari, C. Sieben, A. Benke, D. M. Suter, B. Fierz, D. Mazza, S. Manley, *PLoS Genet.* **2019**, *15*, 1.

[71] X. Jiang, H. Tian, Y. Fan, J. Chen, Y. Song, S. Wang, F. Zhu, C. Guo, L. Zhang, Y. Shi, *Clin. Vaccine Immunol.* **2012**, *19*, 1938.

[72] D. Wang, H. Wang, J. Brown, T. Daikoku, W. Ning, Q. Shi, A. Richmond, R. Strieter, S. K. Dey, R. N. DuBois, *J. Exp. Med.* **2006**, *203*, 941.